Seismic imaging in and around salt bodies

Ian F. Jones[1] and Ian Davison[2]

Abstract

Seismic imaging of evaporite bodies is notoriously difficult due to the complex shapes of steeply dipping flanks, adjacent overburden strata, and the usually strong acoustic impedance and velocity contrasts at the sediment-evaporite interface. We consider the geology of salt bodies and the problems and pitfalls associated with their imaging such as complex raypaths, seismic velocity anisotropy, P- and S-wave mode conversions, and reflected refractions. We also review recent developments in seismic acquisition and processing, which have led to significant improvements in image quality and in particular, reverse time migration. We tried to call attention to the form, nature, and consequences of these issues for meaningful interpretation of the resulting images.

Introduction

Salt movement often results in steeply dipping complex-shaped structures that pose significant challenges for seismic velocity model building and seismic migration. Recent advances in seismic imaging algorithms have permitted imaging of steep structures by exploiting the two-way wave equation using reverse time migration (RTM). With such imaging algorithms, double bounces and turning-wave reflections can be used to image vertical and overturned salt flanks (Hale et al., 1992; Bernitsas et al., 1997; Cavalca and Lailly, 2005; Jones, 2008). However, despite advances in migration algorithms, the derivation of an acceptably realistic earth model incorporating the anisotropic behavior of the velocity field remains a significant challenge, requiring tight integration of geologic interpretation and geophysical skills (e.g., Jones, 2012; McCann et al., 2012). These observations hold true for marine, land, and ocean-bottom cable (OBC) data, but in this paper, we will cover the topics generically.

A major factor in the successful execution of a complex salt imaging project is the understanding of the many and varied pitfalls involved at every stage of the process. Here, we describe and discuss some of these issues, including the following:

1) Our ability to adequately describe geologic reality, addressing large scale and crystalline structure, rheology, and anisotropy. In building a model of any physical system, we must make approximations, so we need to assess if these approximations are acceptable, if they can be improved upon with emerging technologies, and if their consequences give rise to misleading results.
2) Diagenesis and cap rock formation in salt bodies. Often, we oversimplify the salt cap structures, especially if the cap material is thin or confused with flank sediments. This can distort the final image because we would then be using inappropriate velocities in the vicinity of the salt.
3) Stress-induced effects. Sound speed is affected by stress, so measuring sound speed for adjacent sediments can give misleading results if these values are then applied to a stressed region of the same rock type.
4) Acquisition limitations resulting in poor illumination and poor sampling. We seldom, if ever, acquire the data we would like to have, but rather are limited by costs or practicalities. The consequence of these compromises impedes our ability to form a reliable image.
5) Time-imaging interpretation pitfalls. Using images based on inappropriate technology was commonplace historically, but fortunately, contemporary depth imaging can avoid this problem.
6) Complex travel paths associated with salt-related seismic arrivals, one-way versus two-way propagation imaging issues, refraction-related events. The travel paths of sound in the vicinity of complex geometries is very complicated, often making it extremely difficult to make sense of the data we are working with.
7) Inappropriate preprocessing. Many conventional preprocessing workflows were developed in the days prior to the availability of complex imaging algorithms: Judicious use of such methodologies is necessary in the vicinity of complex structures.

[1]ION GX Technology EAME, Egham, UK. E-mail: ian.jones@iongeo.com.
[2]Earthmoves Ltd., Camberley, UK. E-mail: i.davison@earthmoves.co.uk.

Manuscript received by the Editor 21 February 2014; revised manuscript received 23 June 2014; published online 8 September 2014. This paper appears in *Interpretation*, Vol. 2, No. 4 (November 2014); p. SL1–SL20, 28 FIGS., 1 TABLE.
http://dx.doi.org/10.1190/INT-2014-0033.1.

8) Anisotropy representation and parameterization. Most of the time, we do not have sufficient information (measured data) to adequately describe the anisotropic behavior of the subsurface, hence great ambiguity remains concerning anisotropy.
9) Seismic mode-converted events. Contemporary migration theory is still only acoustic. Hence, we ignore the phenomenon of mode conversion, so any such waveforms in the measured data manifest as a class of noise, thus contaminating the final images and parameter estimations.

Many of these issues are interrelated: For example, the current industrial state-of-the-art practice of using acoustic migration (ignoring mode conversion at interfaces) results in treating such energy as noise, which contaminates the image and misleads the interpreter.

Physical properties of evaporites and velocity anisotropy

When a salt model is being built for depth imaging, it is often assumed that the evaporite body is pure halite with a constant compressional wave speed of 4500 ms^{-1}. However, almost all salt bodies contain varying amounts of gypsum ($V_P = 5700$ ms^{-1}) or anhydrite ($V_P = 6500$ ms^{-1}), and some bodies contain significant amounts of K-Mg-rich salts with seismic velocities as low as 3500 ms^{-1} (Table 1). In addition, other factors such as bound water also affect the sound speed. A thick (up to 400 m) anhydrite cap rock can develop over the crest and flanks of a salt diapir due to salt dissolution, which leaves an anhydrite residue (Figure 1). For example, the Epsilon diapir in Norway was initially interpreted as a thin salt stock on time-migrated seismic data, but upon drilling, the stem

Table 1. Physical properties of main evaporite minerals.

Mineral	Composition	Hardness	Density ($kg\,m^{-3}$)	Seismic velocity (ms^{-1})
Halite	NaCl	2.5	2200	4500
Gypsum	$CaSO_4 \cdot 2H_2O$	1.5–2	2300	5700
Anhydrite	$CaSO_4$	3.5	2900	6500
Tachydrite	$CaMg_2Cl_6 \cdot 12H_2O$	2	1660	3500
Sylvite	KCl	1.5–2	1990	4110
Carnallite	$KMgCl_3 \cdot 6(H_2O)$	2.5	1600	3900
Kieserite	$MgSO_4 \cdot H_2O$	3.5	2550	?
Langbeinite	$K_2SO_4 \cdot 2H_2O$	3.5–4	2820	5860
Polyhalite	$K_2SO_4 \cdot MgSO_4 \cdot 2CaSO_4 \cdot 2H_2O$	2.5–3.5	2790	5300
Dolomite	$CaCO_3 \cdot MgCO_3$	3.5–4	2870	6300

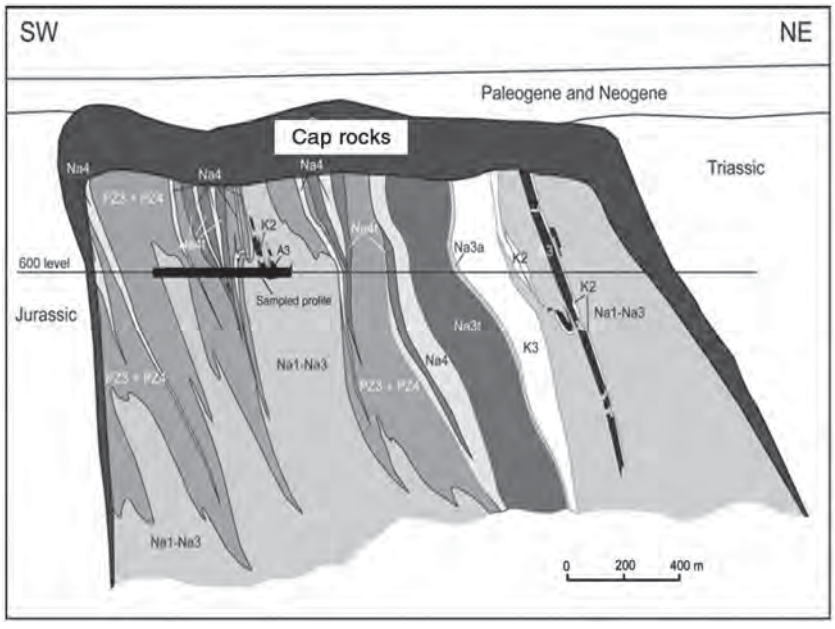

Figure 1. Kłodwa salt diapir in Poland showing a well-developed anhydrite cap rock (seismic velocity of 6500 ms^{-1}) from Burliga et al. (2005).

was found to be much wider and included a ~300–350-m-thick anhydrite flank layer (Jackson and Lewis, 2012; Figure 2). It is recommended that varying velocities are tested in initial velocity model building in areas in which the evaporite composition is unknown. In addition, all deformed salt bodies contain interbeds of different compositions and mineral grains, which are preferentially elongated in the flow direction (Figure 3). This is subvertical in salt diapirs and subparallel to strata in autochthonous salt layers. The ultrasonic P-wave seismic velocity anisotropy (wavelength of less than 1 mm) has been measured at up to 7% faster in the flow direction, in which the raypath crosses fewer grain boundaries (Raymer et al., 1999, 2000). Individual interbeds of anhydrite and dolomite may also increase velocity anisotropy within the evaporite body if they remain as intact layers over large areas. However, it is not known whether the seismic velocity anisotropy of much longer wavelength (10–100 m) seismic waves is impor-

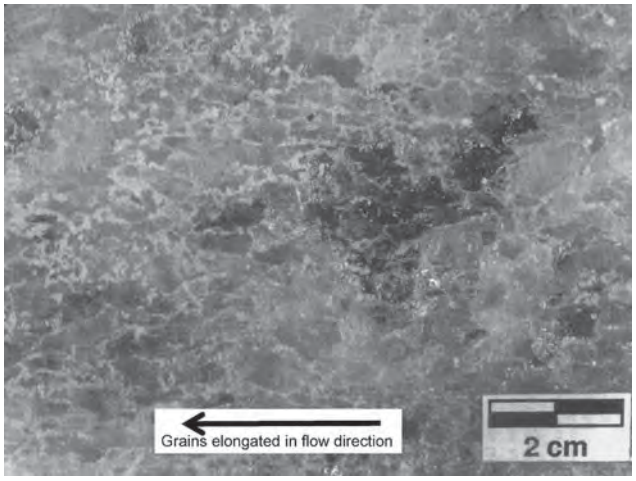

Figure 3. Photograph of deformed halite from the stem of salt diapir in Yemen. Flow direction approximately from right to left (from Davison et al., 1996). Courtesy of the Geological Society of London.

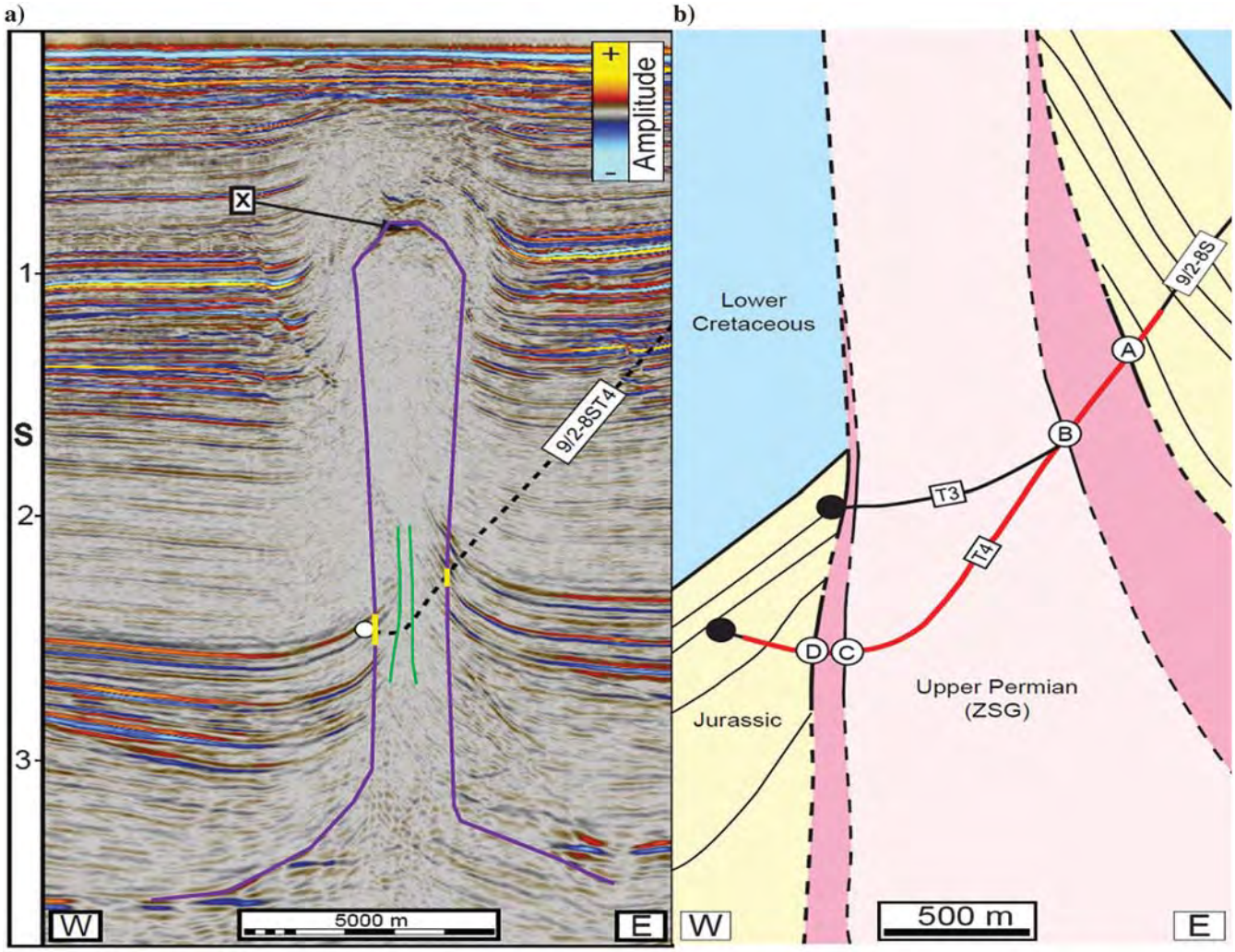

Figure 2. (a) Seismic section through the Epsilon diapir, Norwegian North Sea, showing the predrill interpretation of the width of the salt diapir neck in green and our postdrill interpretation in purple. The yellow bars indicate the control points in the well that intersected the sediment-anhydrite cap rock interface (points A and D in [b]). (b) Detailed line drawing of diapir neck highlighting the anhydrite cap rock in deep pink, salt in light pink. (Jackson and Lewis, 2012). Reproduced with permission from the Geological Society of London.

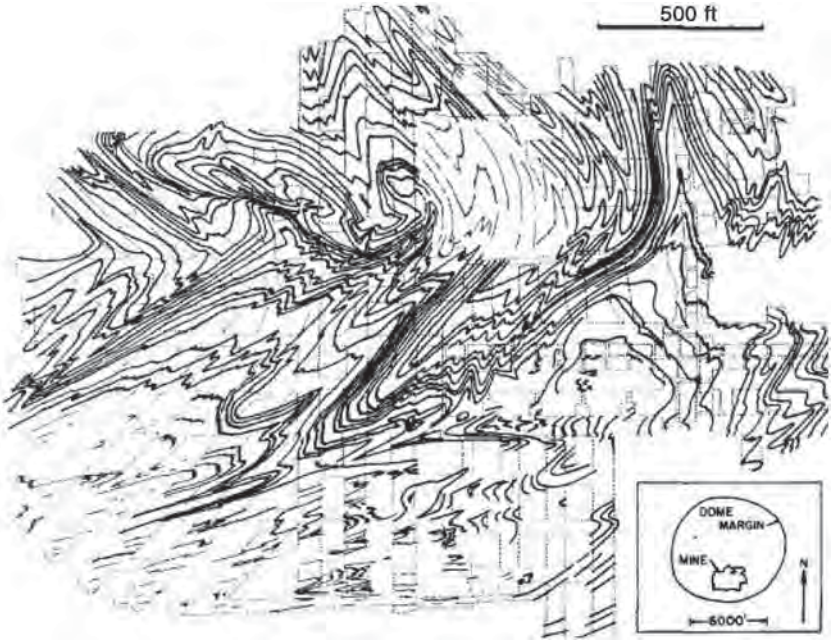

Figure 4. Horizontal plan view of internal folding within the Grand Saline Dome, USA (from Muelhberger and Clabaugh, 1968). Reproduced with the permission of the AAPG.

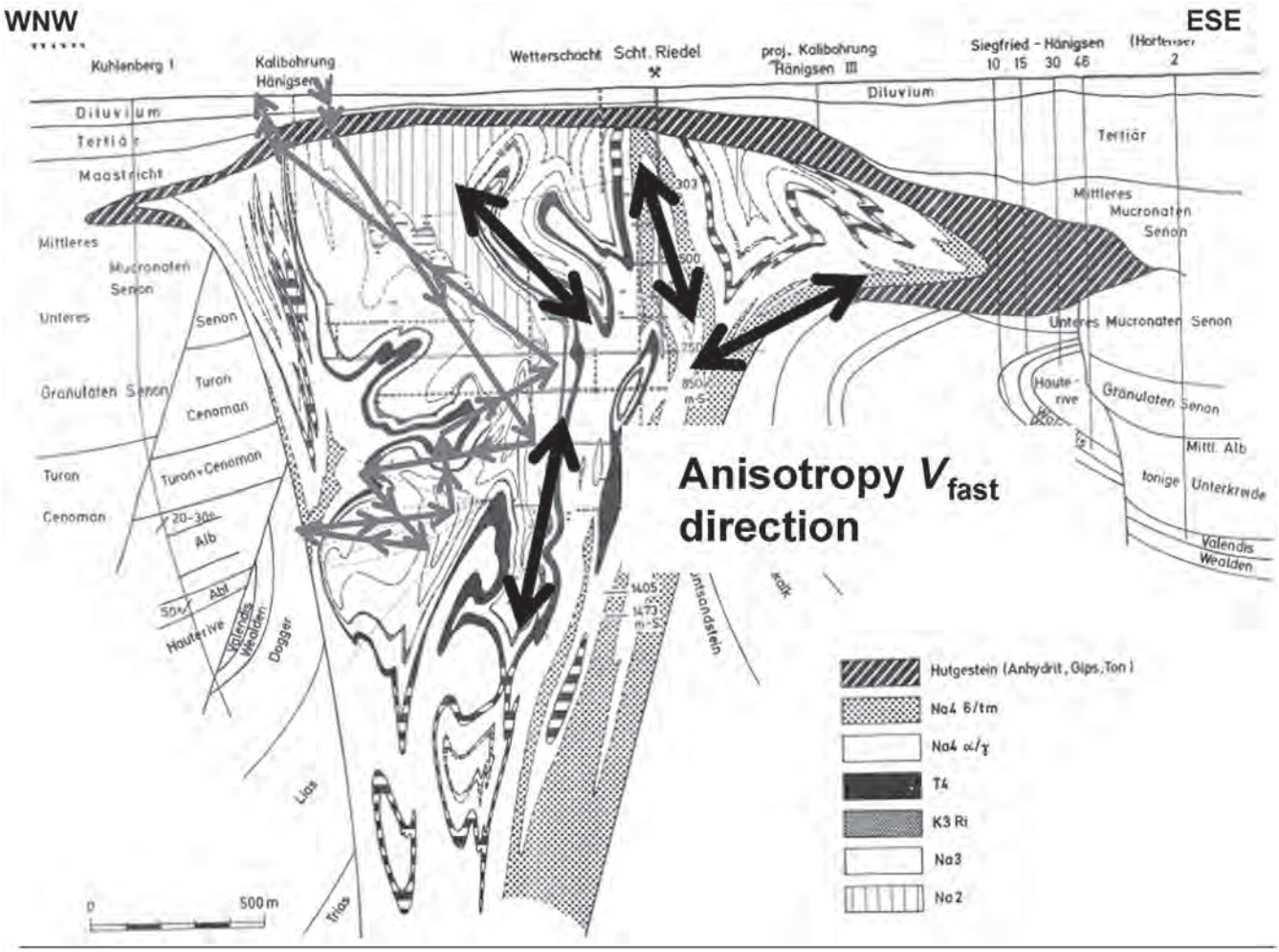

Figure 5. Vertical cross section of the Reidel Salt Dome northwest Germany (from Schachl, 1987). The gray lines indicate the complex repeatedly reflecting raypath that sound may take from a surface source to a receiver during seismic acquisition. The black arrows indicate the localized fast sound speed directions that follow the flow structure.

tant in layered salt bodies. So far, there has been little attempt to incorporate salt anisotropy into velocity model building, and, therefore, this is a possible area for future improvement in seismic imaging.

Internal structures in salt diapirs

When salt flows into a salt body the flow rates vary due to local heterogeneities in the salt and variable salt thickness. Flow instability leads to folding of the salt layers even if there is very little rheologic contrast between layering. For example, differential flow folding is observed throughout the Louann salt in the Gulf Coast of Mexico even when the layering is produced by only slightly higher (4%–5%) dispersed anhydrite content (Figure 4; Muelhberger and Clabaugh, 1968).

The hinge zones of the tight to isoclinal folds within the diapir necks are very steeply dipping (curtain folds) because hinges rotate into the flow direction (e.g., Kupfer, 1976), hence the internal layering is hardly ever imaged, except occasionally at tight fold hinge terminations, in which strong point source reflections are occasionally observed (van Gent et al., 2011). Details of such complex folding can be seen in Figure 5, which shows a vertical section through the Reidel Salt Dome in northwest Germany. The gray lines indicate a "pinball"-like raypath that sound waves could conceivably take within such a complex body. Therefore, it is not surprising that the internal structure of such a body would be extremely difficult to image.

The black arrows on Figure 5 indicate the probable axes of the anisotropic fast direction for the salt body. Such complex anisotropic structures would likewise be very difficult to describe in an anisotropic migration velocity model (e.g., Landrø et al., 2011).

Previous interpretations of seismic data from Brazil's Santos Basin (Figure 6) have suggested that the nonreflective diapir cores are pure halite cutting though layered reflective salts of tachyhydrite, carnallite, and halite. A more likely interpretation would be that the diapirs contain layered strata with intensely folded subvertical axes, which would also explain the lack of reflections in the diapirs. In other words, the poor image quality might not be related to velocity variation resulting only from compositional aspects, but additionally to structural effects. From the imaging perspective, we can still obtain a good presalt image as long as the overall salt velocity variation is captured in the migration velocity model.

Problems and pitfalls with seismic imaging of salt diapirs

Acquisition limitations: Poor illumination

With a complex overburden, not all parts of the subsurface will be equally well illuminated by the downgoing wavefield. In addition, for a subsalt reflection the upcoming wavefield might be postcritically reflected back down at the base salt. Thus, little upcoming energy may actually reach the surface, even though energy reached the subsalt reflector (Cao and Brewer, 2013). Figure 7 shows an illumination study result from a series of uniformly distributed sources on the surface, shooting into a series of uniformly distributed receivers distributed on a 200×200 m grid (this would not be a practical acquisition pattern for a very large real survey, except for moderate sized node or OBC surveys). The geometry of the salt body (Figure 7a) gives rise to a poorly illuminated region at the target location. Even with the very dense shot and receiver layout, the modeling study indicates that it will be difficult to obtain good subsurface illumination in this case. The images obtained from a survey over this feature will be corrupted by migration artifacts in the target zone, so the modeling helps the interpreter to appreciate this problem.

Such analysis of subsurface illumination can help us to design an acquisition program so as to optimally illuminate a given subsurface target. However, it should always be remembered that the conclusions of such studies are specific to the model being used: If the model is significantly in error, then the conclusions may be misleading. In addition, using ray-based methods often gives poor results in complex areas because ray theory assumes that interfaces are smooth on a scale length comparable with the wavelength of the sound illuminating them (e.g., Pratt et al., 1996).

Contemporary acquisition designs such as wide azimuth, multiazimuth and full azimuth (circle shooting) in the marine environment, and dense single sensor deployment in a land (or OBC) environment facilitates enhanced imaging for three reasons. First, having azimuthal variation in the subsurface raypath coverage facilitates better tomographic velocity modeling (e.g., Valler et al., 2012). Second, the improved fold and

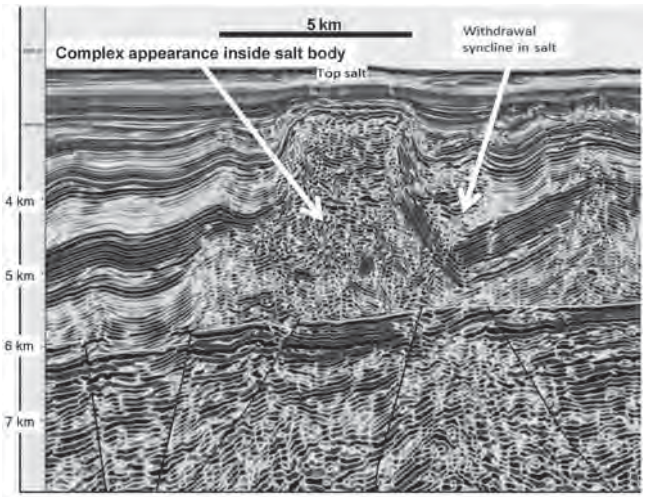

Figure 6. Seismic section through layered salt in the Santos Basin, Brazil. Salt has become diapiric during later salt deposition before any clastic sediment was deposited. The nonreflective diapirs are interpreted to be tightly folded layered salt. The strong reflections within the evaporite body are due to large acoustic impedance contrasts between halite, carnallite, and tachyhydrite (from Davison et al., 2012, reproduced with permission of the Geological Society of London).

azimuthal coverage provides better subsurface illumination, leading to the third point of better noise cancellation (especially of diffracted multiples) and improved imaging. Conventional narrow azimuth acquisition tends to leave coverage gaps in the subsurface over complex targets resulting in poorly imaged data with greater noise content.

In addition, use of longer offsets greatly enhances the chances of better illumination, but more importantly increases the velocity resolution via increased moveout discrimination in the prestack gathers. This in turn helps to better define the model itself.

Time migration pitfalls

With a time migration (or even a rudimentary depth migration such as a constant velocity phase shift technique combined with interpolation), reflections from beds adjacent to salt diapirs are poorly imaged due to the algorithm being unable to correctly handle distortion of raypaths passing though the salt. The time-migrated seismic image shown in Figure 8, has the original interpretation as a narrow stemmed salt body with a bulbous head. On subsequent drilling, it became evident that the salt walls extended laterally beyond the well track, as the drill path and the side track were within salt down to the total depth of penetration. Such misleading images come about in the following way, as described in Figure 9. A tabular salt body may manifest with (correctly) flat lying sediments abutting a poor quality data zone in the raw unmigrated stacked data. Upon time migration, however, the terminations of the sediments swing in and upward to the poor data zone,

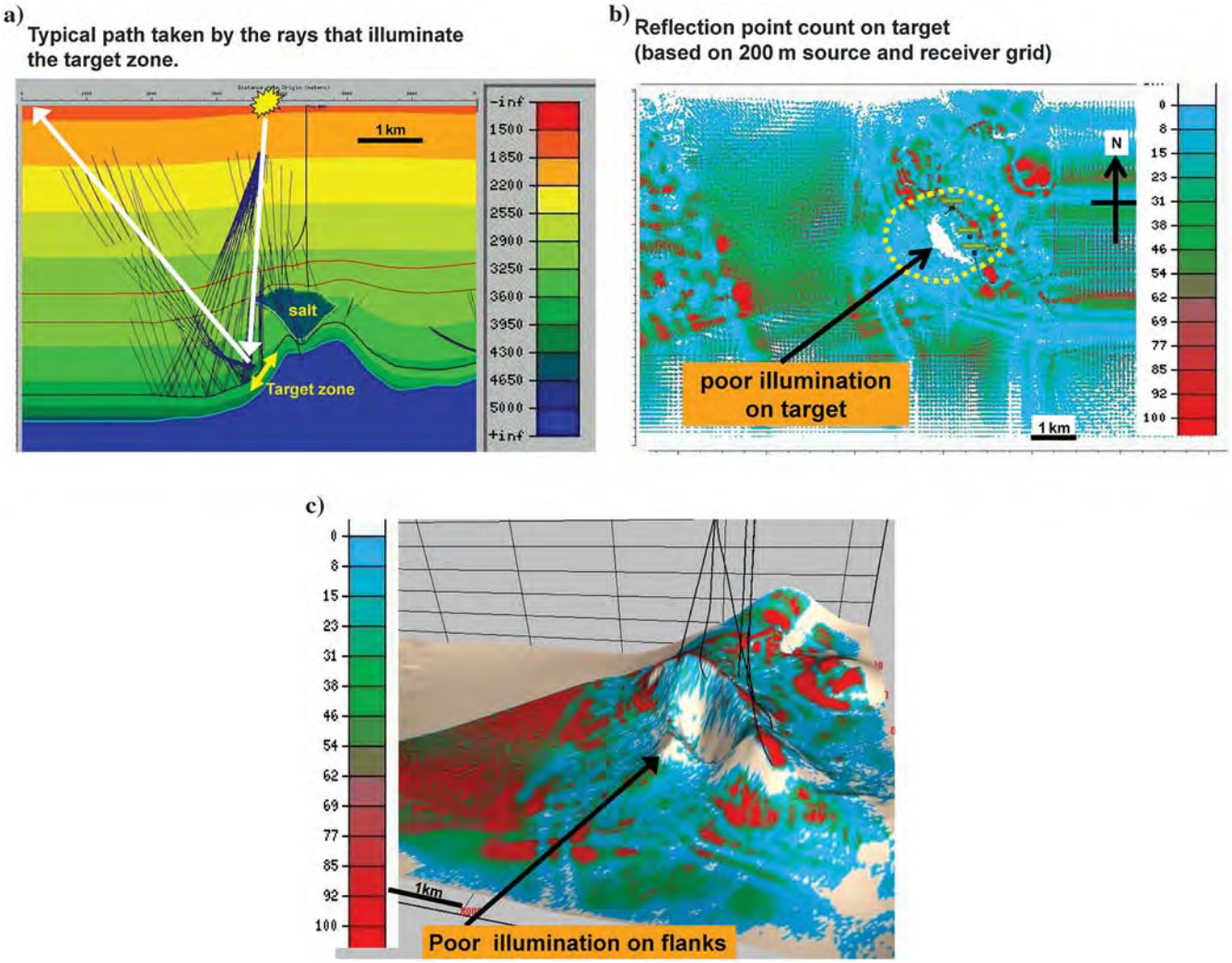

Figure 7. Three-dimensional ray-trace modeling with dense regular acquisition at a 200-m inline and crossline spacing for sources and receivers, for a salt model. (a) Even with this regularly sampled dense acquisition effort, the salt geometry gives rise to poor illumination at target level (the gaps in the rays are due to them being 3D raypaths shown just where they intersect this 2D vertical section), (b) the map view of the ray-trace hit-count gives an indication of likely illumination, which is poor in places. The yellow dotted circle denotes the approximate location of the overlying salt body, and (c) selecting the appropriate subsets of shots and receivers permits emulation of the existing acquisition pattern over this field, and gives the flexibility to consider alternative survey designs for new shooting. Images courtesy of Mike Goodwin, GXT.

giving the appearance of steeply dipping beds, abutting a narrow salt neck. This interpretation pitfall can be commonplace with older time-migrated data, or on non-RTM depth images with inadequate models, hence many diapirs were incorrectly interpreted as teardrop shapes.

For raypaths through a salt body, we also have the potential to obtain highly misleading images when either the model is incorrect, or an inappropriate algorithm is used. Figure 10 shows one such seismic example, in which a salt diapir with a stem, but no base (other than the deep autochthonous salt) was elastically modeled and then migrated with the perfect model, using a conventional (non-RTM) imaging scheme. Some of these complex raypaths are indicated in the figure (e.g., the upturned refracted reflection indicated by the yellow raypath in Figure 10a, and some converted arrivals are shown in Figure 10b). When migrated inappropriately, complex arrivals in the data (such as double bounces and through-salt reflection travel paths) can produce what appears to be a false "base salt" in the diapir image. In Figure 11a, conventional migration of these synthetic data produced a false allochthonous base-salt image and a similar result is observed on the real North Sea data example shown in Figure 11b (Jones et al., 2006). Subsequent migration of these data using RTM with an appropriate velocity model produced an image with the salt stem (Farmer et al., 2006).

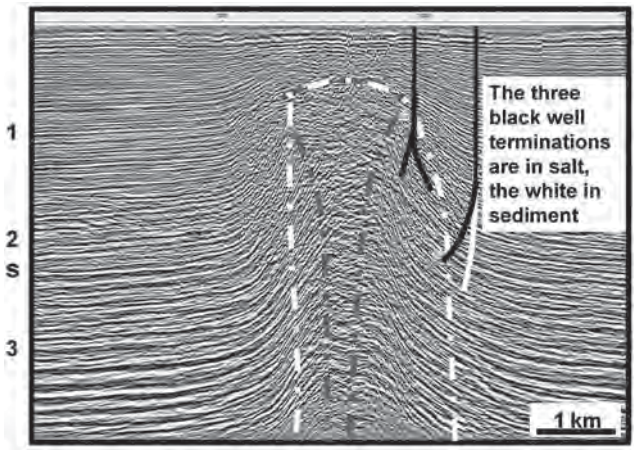

Figure 8. Seismic section through a salt diapir offshore West Africa showing a tear drop predrill interpretation (gray dashed line) based on drawing though the terminations in seismic reflections. Four well bores are shown, three of which drilled into the salt diapir and remained in salt. The white dashed line is the preferred postdrill interpretation of the salt diapir shape. Seismic image courtesy of Svenska Petroleum Exploration AS.

One-way versus two-way depth imaging

In the solution of the wave equation, a square-root term has to be evaluated. However, a square root has a positive and a negative solution. Geometrically, these two roots correspond to the downgoing wavefield emanating from the source and the upcoming wavefield reflected from an impedance contrast in the subsurface and detected by the receivers (Figure 12). In conventional imaging of seismic data, we assert that we are only interested in the upcoming wavefield after a single reflection in the subsurface, hence we only solve for one of the two square roots. This is called a one-way solution of the wave equation. As indicated in Figure 12, there are occasions when we need to deal with energy that propagates in both directions on its path from the source to the reflector, or from the reflector back toward the surface. In this case, we need a two-way solution of the wave equation, such as that offered by RTM for the model building and the migration (see, e.g.,

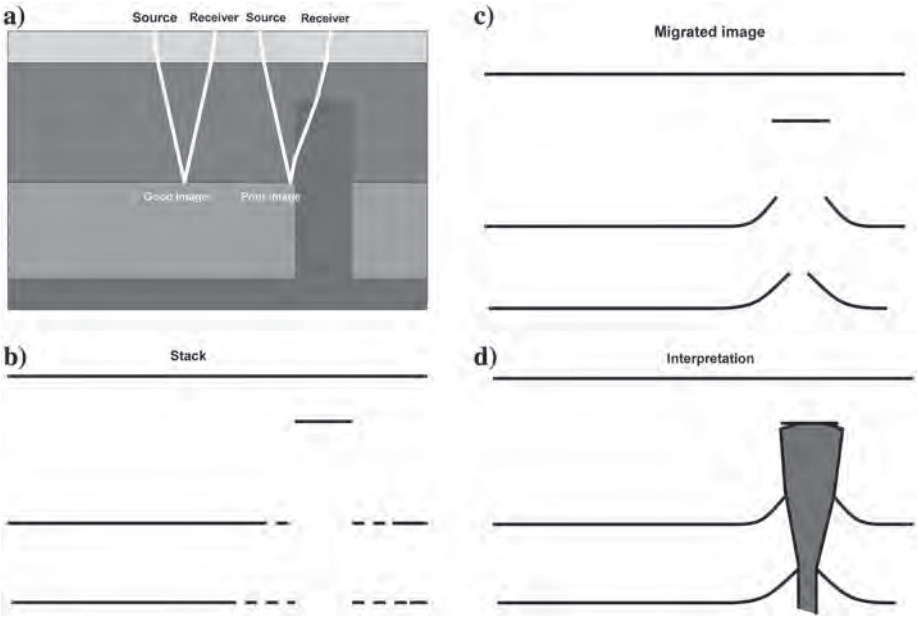

Figure 9. Explanation of the false teardrop shape often produced on interpreted time-migrated seismic sections. (a) Conceptual model showing raypaths away from and near to the salt, (b) stack of poor quality but free from migration distortion, (c) migration "swing" artifacts give a false impression of the salt shape, and (d) misleading interpretation (courtesy of D. Waltham, personal communication, 2013).

Hemon, 1978; Beysal et al., 1983; McMechan, 1983; Whitmore, 1983; Leveille et al., 2011).

The imaging condition in shot migration

In a contemporary shot-based migration (such as RTM), we form the image by propagating a representative source signature down into the earth through the velocity depth model, and at the same time, reverse propagating the recorded surface seismic data back from the receiver locations into the earth through the same model. At each time (or depth) step in this propagation, the two wavefields are typically multiplied together at each coincident point in the earth model: the reasoning being that if a reflector really exists in the subsurface, then at that point in space the downgoing and upcoming wavefields must the in that place at the same time (Claerbout, 1985). The contributions from these products at all time steps are summed to yield the image contribution for this particular shot record (the "convolutional" imaging condition: e.g., Faye and

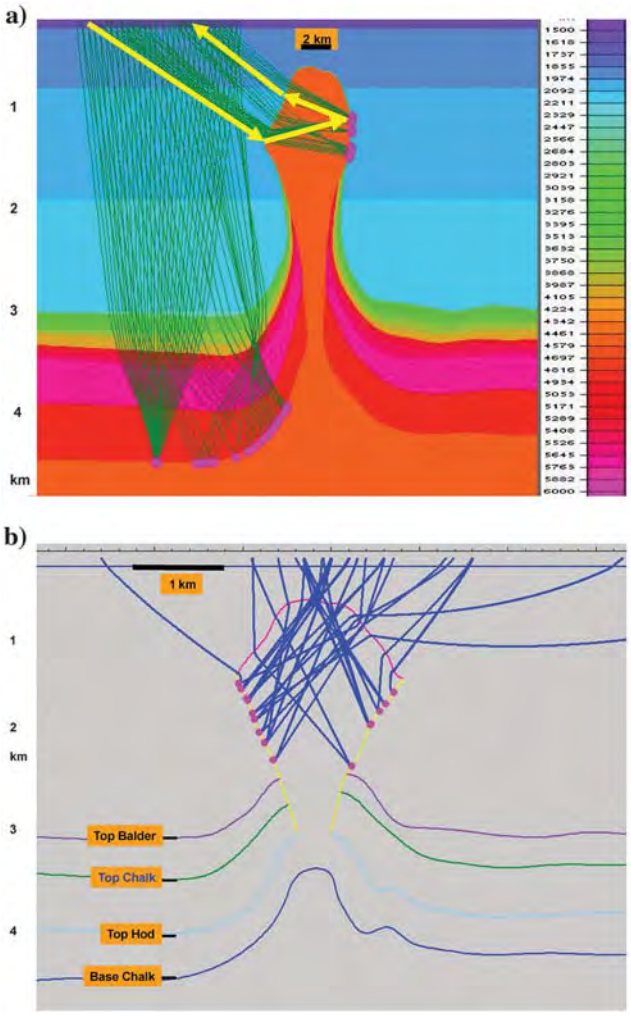

Figure 10. (a) The yellow line indicates a raypath for upward turning refracted reflections within salt and (b) PSSP mode converted internal salt reflections. Purple dots indicate the incident points at the salt interface for these raypaths.

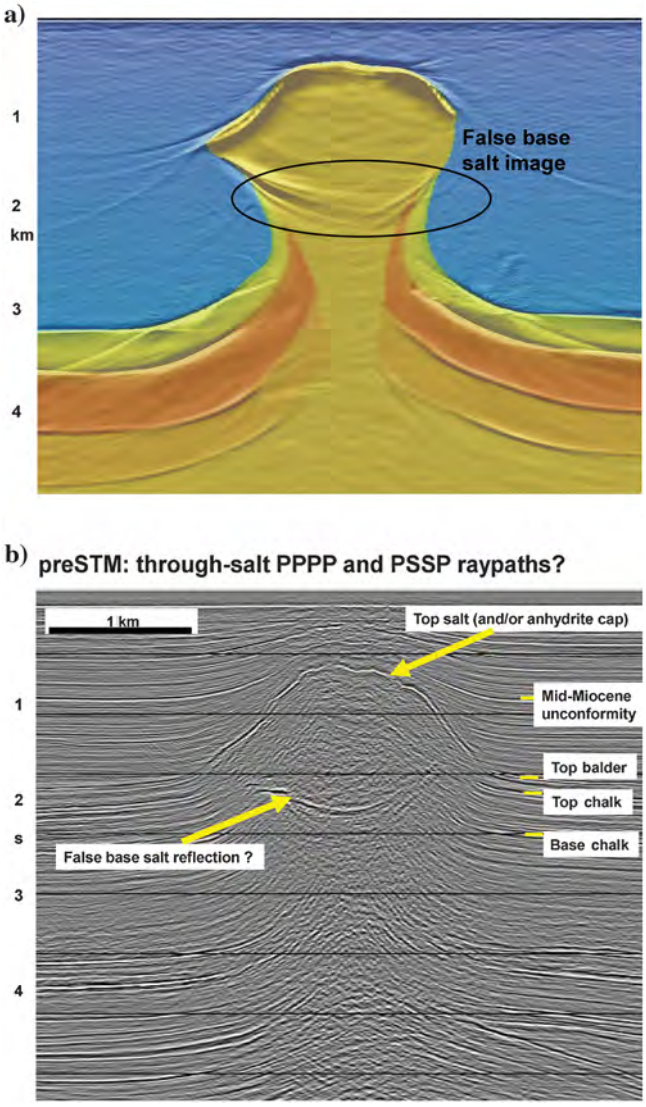

Figure 11. (a) Synthetic elastic modeling results for conventional Kirchhoff migration of a salt body without a base salt in the model. The image gives a false base salt reflection, and panel (b) shows corresponding real data result.

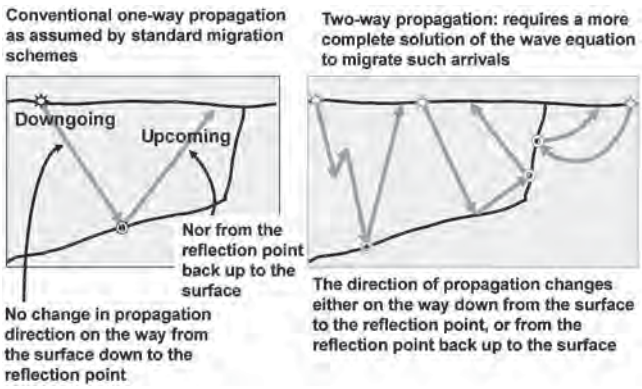

Figure 12. (a) A one-way raypath is one that does not change direction vertically between the surface and the reflector. A simplified migration scheme can be used to image such raypaths and (b) raypaths with a vertical change of direction can in principle be imaged using RTM (from Jones, 2010).

Jeannot, 1986; Rickett and Sava, 2002; Sava and Fomel, 2003, 2006; Zhou et al., 2006; Liu et al., 2011; I. F. Jones, personal communication, 2014).

For a one-way solution of the wave equation, this procedure leads to an image of any simple reflections (Figure 13). For a two-way solution, the source-side forward propagation and the receiver-side backward propagation can travel upward and downward (in other words, a two-way solution permits a change in vertical direction during propagation). This permits imaging of steep and complex geobodies via exploitation of double bounces and turning rays (e.g., Hale et al., 1992; Bernitsas et al., 1997; Cavalca and Lailly, 2005) but also results in some unwanted side effects described in the following section. Figure 14 indicates how and where these unwanted contributions can form.

Reverse-time migration imaging artifacts

The benefit derived from RTM imaging results from its ability to fully comprehend the upcoming and downgoing components of the seismic wavefield. Unfortunately, without using relatively computationally expensive filters during the migration (e.g., Yoon et al., 2004; Yoon and Marfurt, 2006), forming the image from the upcoming and downgoing two-way-propagated wavefields can result in spurious strong near-vertical artifacts (e.g. Loewenthal et al., 1987; Fletcher et al., 2005; Guitton et al., 2006). These can be caused by lateral amplitude terminations (localized edge effects) on strong vertical velocity boundaries, from laterally mispositioned double-bounce arrivals (e.g., when we have significant error in the anisotropy parameters) and also from the migration of reflected refractions.

An example of such an artifact is shown in Figure 15: The near-vertical strong event emanating from the left flank of the salt dome is clearly nongeologic. After filtering of the RTM prestack angle gathers this event can be suppressed. This class of event is most likely a result of the class of artifact shown in Figure 14.

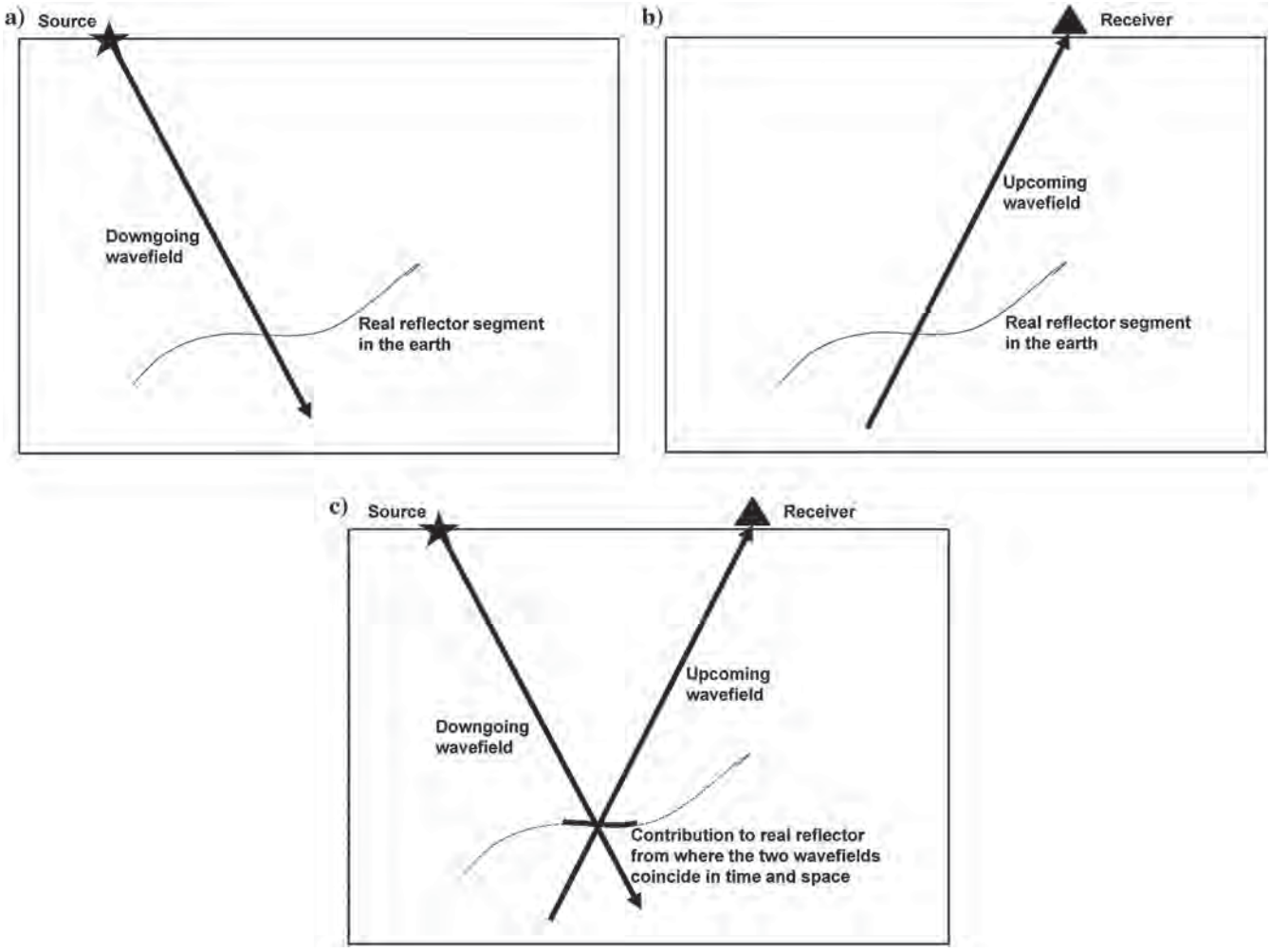

Figure 13. One-way shot migration imaging condition for a simple reflector. (a) Downgoing source-side wavefield for one-way propagation (the wave can travel down into the earth, but never back up), (b) upcoming receiver-side wavefield (the wave can travel up toward the surface, but never back down), and (c) imaging condition from multiplying both wavefields together to form a contribution to the final image.

Pitfalls of one-way migration of two-way raypaths

Although RTM is now the algorithm of choice for dealing with data from complex salt provinces, it is instructive to describe what happens to energy in the seismic records resulting from propagation on double-bounce (prism) wavepaths or to continuously refracted (diving or turning) wavepaths, if we migrate these data with a conventional one-way migration scheme.

Figure 16 shows two images of a west African salt body migrated using the same data and velocity model, but with a two-way propagator (RTM) and a one-way wave equation migration (WEM) propagator (in this case, a split-step Fourier plus interpolation). The conventional (one-way) migration WEM algorithm does not correctly comprehend the energy traveling on the white double-bounce raypath, but rather treats it as if it had the same total travel time and similar source and receiver emergence angles. It also creates an artifact event, where this fictitious one-way raypath would have been (gray raypath). In mispositioning the double-bounce energy in this way, the WEM algorithm creates a new class of noise that confuses the image, so it is not just the case that the steep salt flank reflector is missing, but that any useful parts of the image are further contaminated by this new misleading noise.

How complex can salt-related seismic arrivals be?

To give some idea of how complex the returned seismic wavefield can be, even for a "simple" tabular salt wall (Figure 17), we have conducted some acoustic finite-difference 2D modeling. In the model, a salt wall, 4.4 km from the shot location, sits above a flat lying high-velocity contrast layer (chalk) at 3-km depth. The velocity contrast at the layer is 2:1.

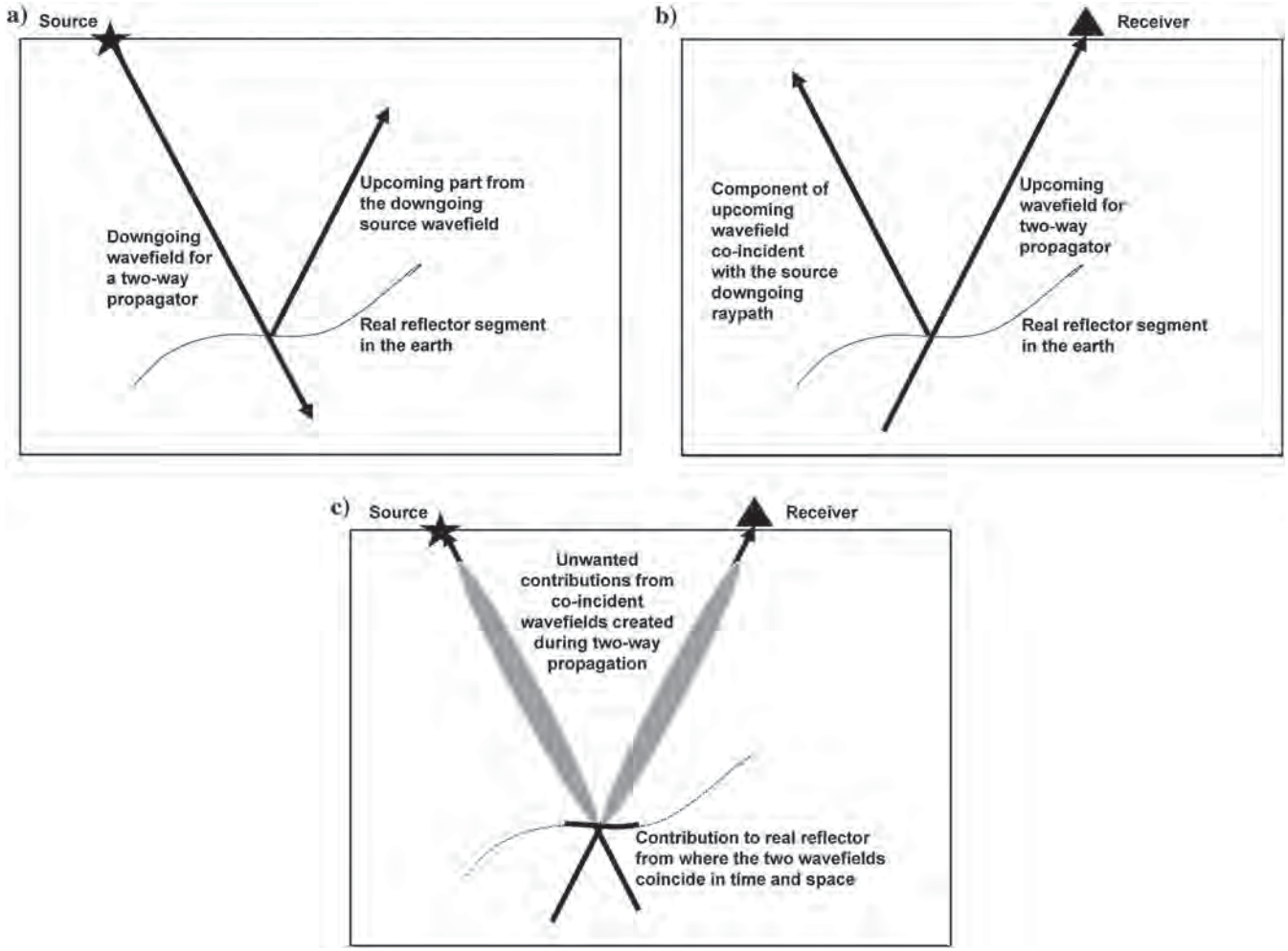

Figure 14. Two-way shot migration imaging condition for a simple reflector. (a) Downgoing source-side wavefield for two-way propagation — this has energy on the downgoing path, but also creates a contribution backup along the upgoing path (in other words, unlike one-way propagation, it can travel downward and upward), (b) upcoming receiver-side wavefield propagated back into the earth toward the reflector also reflects back upward toward the source (as with the source-side term, the receiver-side energy can travel upward and downward), and (c) imaging condition from multiplying both wavefields together to form a contribution to the final image, but we also get an unwanted image contribution that has to be removed.

In Figures 17 and 18, we show sketches of various raypaths, for the simplest single bounce at the flat reflector, various double-bounce reflections, scattered arrivals from the salt edges some of which are subsequently reflected, and also refractions which later reflect and even undergo a second reflection. This plethora of events gives rise to a very complex shot record (Figure 19), with the various arrivals indicated. For real data, this situation would be far more complex because the geometry would not be simple and we would also have converted mode arrivals (albeit often with a lower amplitude than the P energy). Mode converted arrivals will be present for land data and perhaps surprisingly, for shallow water marine data, in which upcoming mode converted S-wave energy converts back to P at the sea bed (Jones, 2013).

Refracted energy

Another source of spurious reflections is produced by reflected-critical refractions along stratal boundaries adjacent to steep salt bodies, in which a false "Christmas tree"-like structure and other effects can be produced. This phenomenon was discussed extensively in the early seismologic literature (e.g., Brauch, 1958). Depending on the relative geometry of the flat-lying sediments and the abutting near-vertical salt body, there are several possible artifact-generating mechanisms. For example, if a stratal reflector meets the salt wall perpendicularly, then downgoing energy that has been critically refracted along the sediment interface will reflect straight back off the salt wall and travel back along the flat lying horizon. In this case, the refraction energy will propagate back to the surface as a head

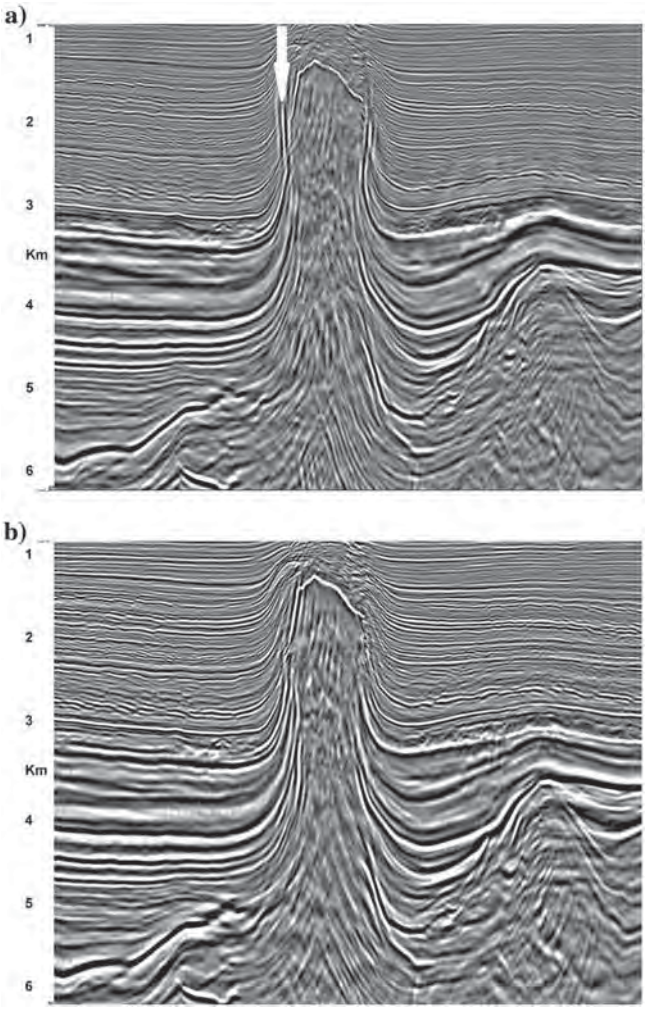

Figure 15. (a) Near-vertical RTM artifact emanating from a strong reflector termination, indicated by the arrow. This image is taken from an earlier stage of the velocity model building and (b) image from later stage in the model building after filtering of RTM angle gathers (GXT RTM image shown courtesy of Talisman Sinopec Energy UK and partners GdF-Suez, EON, and Idemitsu. Input data courtesy of CGG).

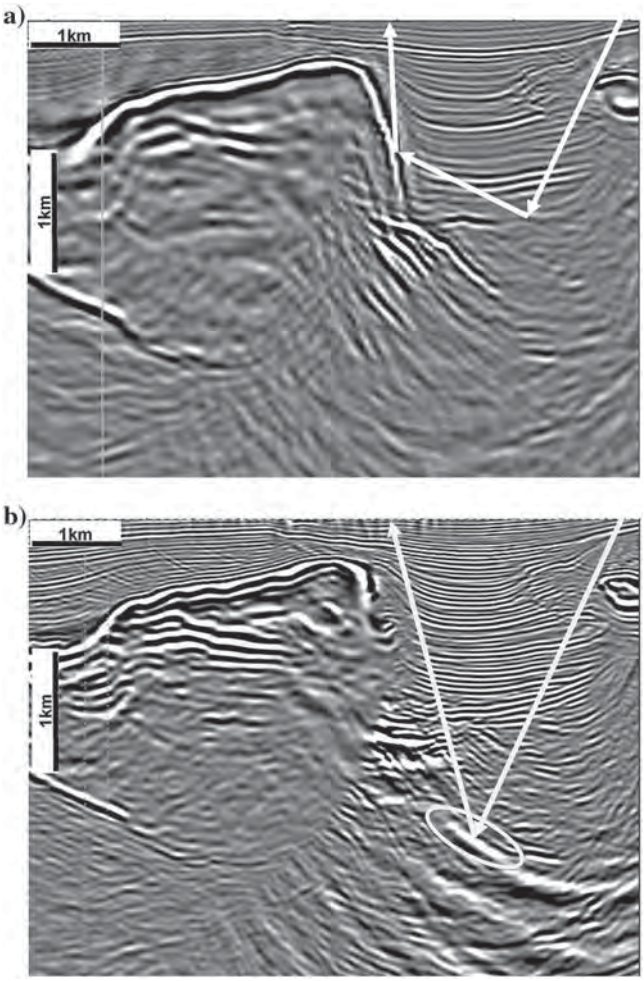

Figure 16. (a) RTM image of west African salt body. RTM can correctly image two-way double-bounce arrivals (white raypath) and (b) a conventional (one-way) migration WEM algorithm does not correctly comprehend the energy traveling on the orange raypath, but rather treats it as if it had the same total travel time and similar source or receiver emergence angles (the gray path) and creates an artifact event, where this one-way raypath would have been (indicated by the ellipse).

wave traveling on the same path as the downcoming wave, but in the opposite direction (Figure 20a).

In addition to raypath (i) shown in Figure 18, Figure 20b describes other possibilities for reflected refractions where dipping strata meet a salt wall. An upcoming head wave undergoing a reflection from the salt wall, can produce arrivals that look like legitimate double-bounce reflections. In this geometry, legitimate double-bounce reflection events can occur for a range of incident angles (not just the critical angle) as indicated in the black raypath; but we also have the spurious events (indicated by the blue raypaths) for locations ranging from the intersection of the reflector with the salt wall and up along the salt wall itself where the head wave reflects off the salt. These blue raypaths will produce confusing features in the RTM image. In practice, it will be very difficult to distinguish which raypaths happen to give rise to a particular observed

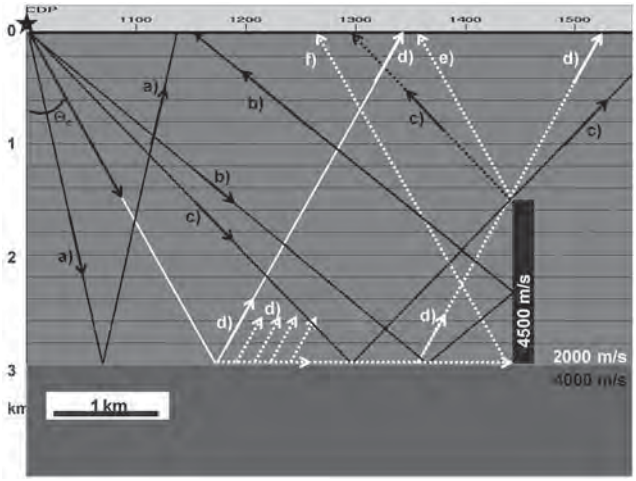

Figure 17. A simple velocity model with a single flat lying reflector and a vertical tabular salt wall. The source at the left is located 4.4 km from the salt wall, and the maximum receiver offset is 9 km. Various possible raypaths are shown. (a) Simple reflection of the flat layer, (b) double bounce from the flat and vertical interfaces, (c) limiting case for the farthest double bounce and simple reflector, (d) upcoming head wave, (e) upcoming head wave after reflection from the vertical salt wall, and (f) nearest reflected refraction.

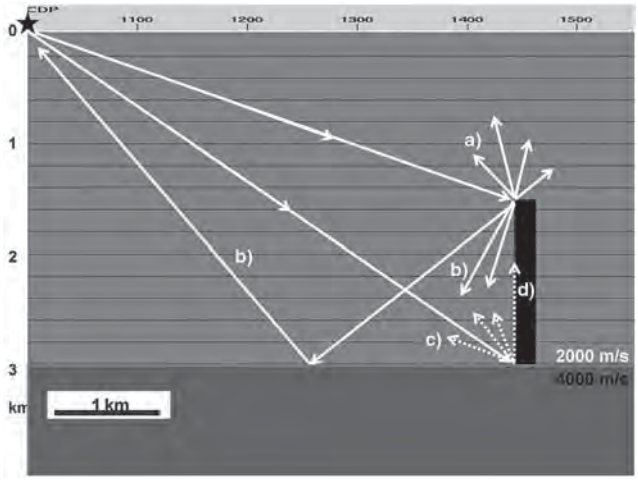

Figure 18. Additional raypaths in the simple salt model (labels continue from Figure 17 and correspond to Figure 19): (g) Upcoming scatter at the top salt corner from downgoing direct energy (we also have similar scatter from upcoming double-bounce arrivals), (h) downward scattered energy reflecting back up from the flat reflector, (i) base salt corner upcoming scatter, and (j) base salt upcoming scatter traveling in the salt.

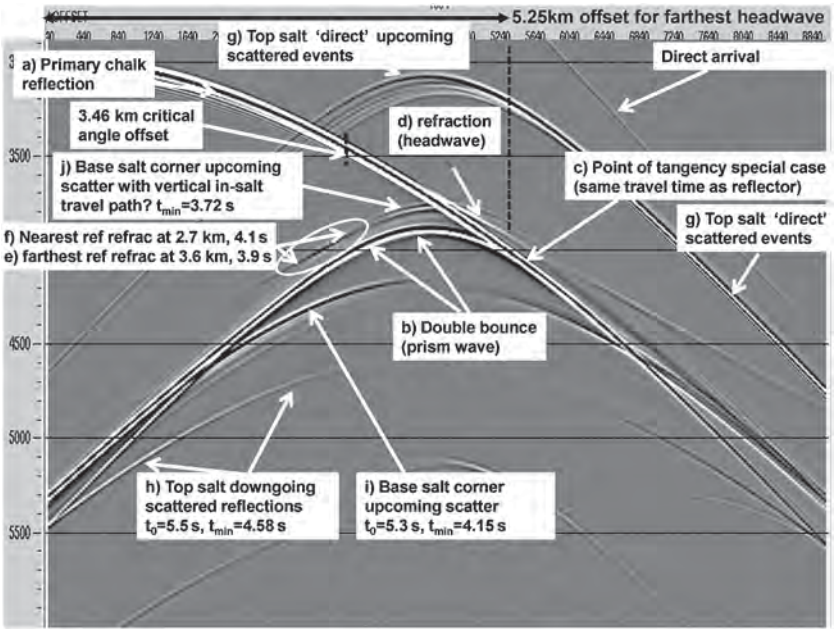

Figure 19. Events in the shot record corresponding to the raypaths outlined in Figures 17 and 18. (a) Simple reflection of the flat layer, (b) double bounce from the flat and vertical interfaces, (c) limiting case for the farthest double bounce and simple reflector, (d) upcoming head wave, (e) upcoming head wave after reflection from the vertical salt wall, (f) nearest reflected refraction, (g) upcoming scatter at the top salt corner from downgoing direct energy (we also have similar scatter from upcoming double-bounce arrivals), (h) downward scattered energy reflecting back up from the flat reflector, (i) base salt corner upcoming scatter, and (j) base salt upcoming scatter traveling in the salt.

feature in an RTM image. Fortunately, they often have weak amplitudes.

Preprocessing considerations for reverse time migration

In addition to the migration, we must also consider the preprocessing procedures used prior to migration. Conventional processing strategies have traditionally been designed for one-way propagation, hence many conventional approaches to preprocessing can damage or entirely remove two-way energy from the data, thus limiting the potential of a subsequent RTM (e.g., Jones, 2008). This is because double-bounce reflections, turning rays, and through salt reflections often appear the same as backscattered noise when seen in CMP gathers, and, thus may be inadvertently removed in a traditional preprocessing flow. Figure 21 shows a salt wall velocity model (based on a real scenario) and

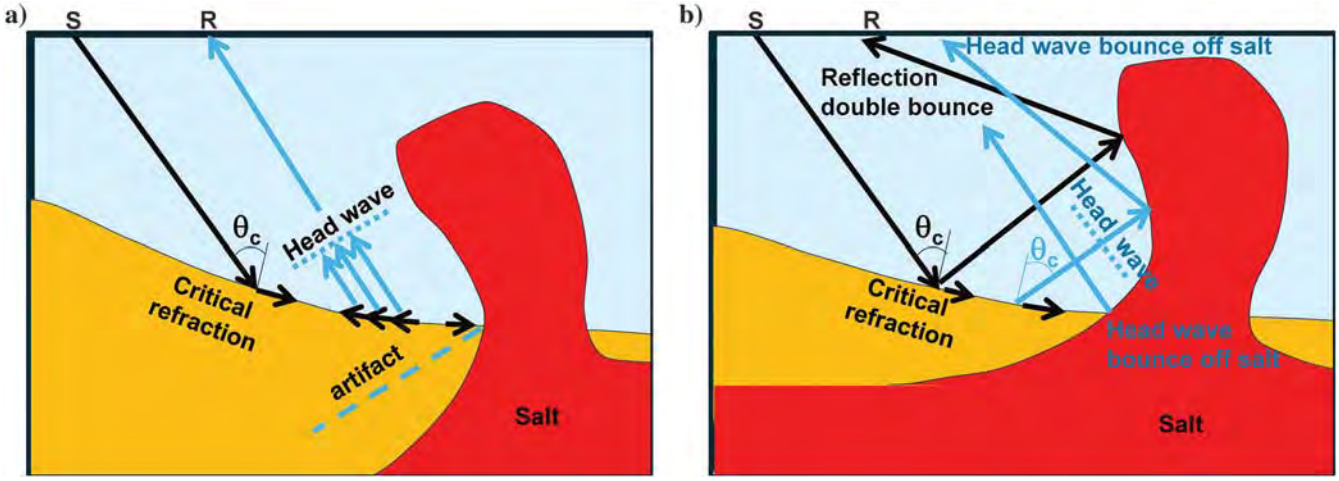

Figure 20. (a) Raypath of reflected-critical refraction from a diapir wall for downgoing waves from source location S and receivers R. The upcoming head wave seen at the receivers will produce a straight apparent reflection artifact emanating from the intersection point of the reflector with the diapir wall producing an apparent Christmas tree feature (dashed blue line) (D. Waltham, personal communication, 2013) and (b) head wave undergoing a reflection from the salt wall produced arrivals that look like legitimate double-bounce reflections. In this geometry, we will have legitimate double-bounce reflections (the black raypath), and also spurious events (in blue) for locations ranging upward from the intersection of the strong reflector with the salt wall, in which the head wave reflects off the salt. These blue raypaths will produce confusing features in the RTM image.

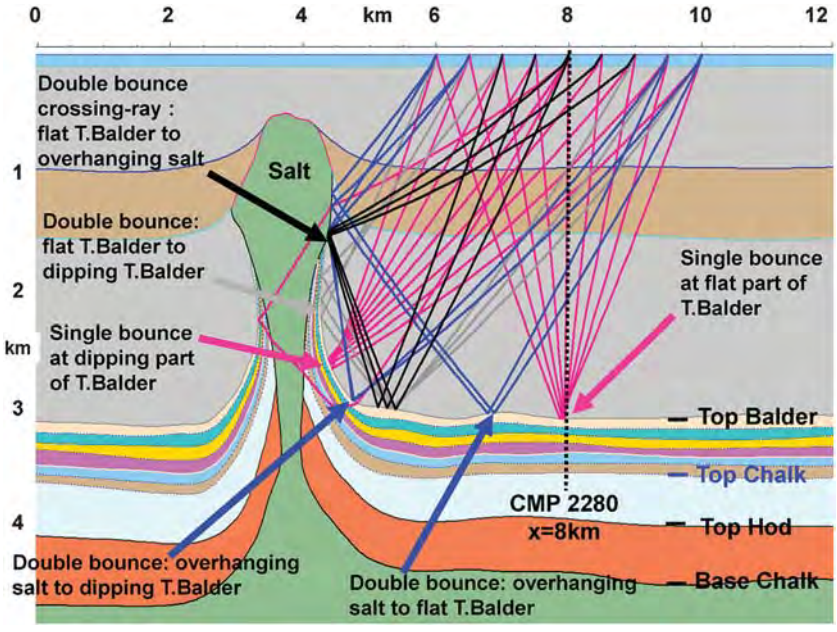

Figure 21. Plot of a few sparse rays shown against the interval-velocity model. The sediment P-wave sound speed ranges from approximately 1900 to 2200 ms^{-1}, with some shallow impedance-contrast events. The absence of a strong sediment gradient precludes turning rays in the sediments, whereas a strong compaction velocity gradient below the top Balder and top Chalk does produce turning rays. The salt velocity (green) is 4500 ms^{-1}, the upper chalk velocity is approximately 5700 ms^{-1}, and the lower chalk velocity is approximately 4900 ms^{-1}.

double-bounce raypaths reflecting from the flat-lying sediments and the salt wall (Jones, 2008). The 2D synthetic CMP gathers associated with this model are shown in Figure 22a, where it can be seen that the moveout behavior of these data does not conform to the usual hyperbolic assumptions of conventional preprocessing. Figure 22b shows the CMP gathers after some conventional and often-used preprocessing, namely muting in the *tau-p* domain (as routinely done during short-period *tau-p* deconvolution), and also an apex-shifted multiple suppression technique (designed to remove scattered multiples). Figure 23 shows an RTM image with and without this conventional processing route; the former significantly damages the image.

Structurally induced velocity anomalies

The state-of-the-art in velocity model building rarely, if ever, permits us to characterize the anisotropy within a salt body, but currently, we are able to use a tilted transversely isotropic (TTI) representation of the adjacent and overlying sediments. In a TTI representation, and especially for shaley materials, the fast velocity direction is nominally parallel to, and the slow direction perpendicular to, the bedding planes. However, this assumes postdepositional deformation and compaction. In reality, there is often some degree of syn-depositional deformation and, therefore, the polar angle for the TTI will be at some intermediate angle between the vertical and the structural bedding angle. Some workers have recently been using a polar angle set to be (arbitrarily) half the structural angle, but this is not necessarily the real situation. Figure 24 shows this with a series of sketches: The orientation of platy minerals will parallel the underlying bedding (as will the mineral orientation of any diagenetic mineralization). If the layers are subsequently deformed, then the polar axis of the mineral grains will still be conformable to the bedding axis. However, if the underlying strata are being continuously deformed during deposition, then the grains will initially be deposited locally flat lying with a vertical polar axis. This will then be tilted by further ongoing deformation.

In cases where we have well-defined stress-induced fractures perpendicular to the bedding planes (e.g., Davison et al., 2000), the simple TTI description will fail (as the fractures may result in a reduction of the sound speed in the nominally fast direction) and we have to superimpose another notion of a fast and a slow direction related to the fracturing within the layers. So the TTI description for the tilted layering needs to be modified to accommodate intralayer fractures. This can be taken into account using an orthorhombic description of the anisotropic behavior — in other words, a description that assumes two orthogonal directions governing the sound speed, rather than just one, as in a TTI description (Figure 25). Several recent case studies have shown improved imaging in the vicinity of salt bodies by taking stress-induced crestal fracturing into account using orthorhombic migration (e.g., Li, 2012; Zdraveva, 2012). Current industrial practice tends to deal with azimuthal anisotropy as a separate phenomenon after a TTI migration of the data has been performed: This can be thought of as a factorized two-pass treatment, rather than the more correct orthorhombic treatment (e.g., Valler et al., 2010). A complete description of anisotropic behavior, combining the layering (TTI) effects with fracture-related effects, in which the fractures could be at arbitrary angles to the TTI polar axis, would be described as triclinic anisotropy. That is well beyond our ability to characterize, however, as we have insufficient information to do so. Current practice with TTI anisotropic migration requires seven parameters: the structural dip and azimuth, the anisotropy polar dip and azimuth, velocity, and Thomsen parameters epsilon and delta. It is unlikely that we can derive these seven parameters

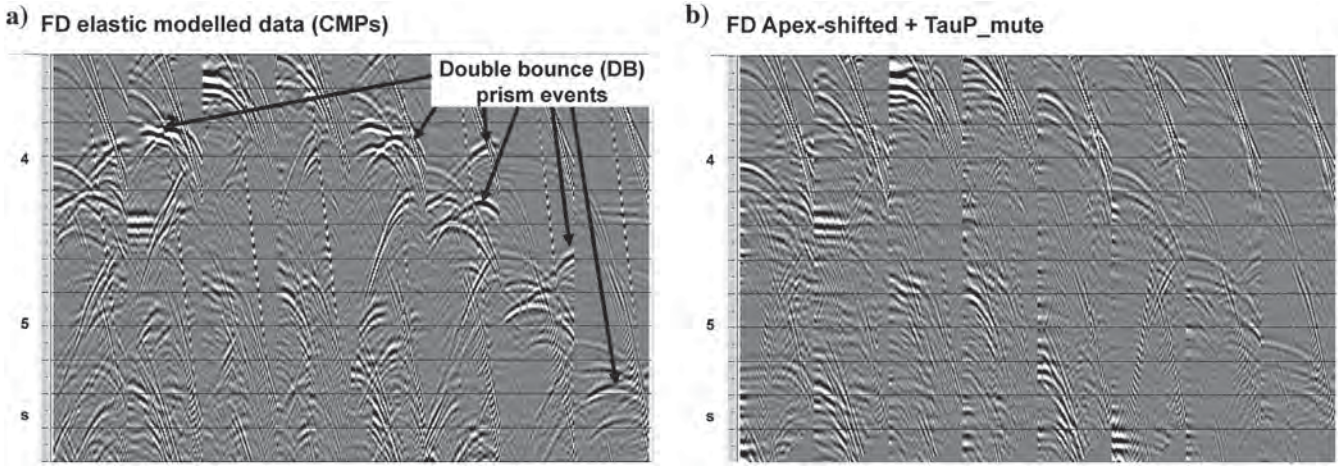

Figure 22. (a) Selection of regularly spaced 2D modeled CMPs with 6 km maximum offset and (b) CMP gathers output from *tau-p* muting and apex-shifted multiple suppression. Apex-shifted events are attenuated successfully: Such event suppression would be considered favorably for conventional processing.

from surface seismic data and well control, consequently, we usually assume that the polar axis is tied to the structural axis; that the delta values determined at a well can be applied throughout the entire 3D image volume and often that epsilon is proportional to delta.

Wave mode conversion

For conventional marine streamer acquisition, we do not usually expect to see shear-related energy because S-waves cannot propagate through the water. However, for geobodies with certain geometries, velocity contrasts and anisotropy, we can have significant wave mode conversion for the downgoing and upcoming wavefields (e.g., Jones, 2013). Hence, for salt bodies, we need to concern ourselves with PSSP and PSPP/PPSP arrivals for two reasons: first, because energy propagating and converting through these different mode paths will contaminate a conventional image (Figure 26; Lafond et al., 2003). Second, if we migrate the data using S-wave velocities in the salt geobody, we can sometimes obtain a useful shear image of the base salt (e.g., Lewis, 2006). This can facilitate better interpretation of the base salt in the velocity model, especially as the incidence angles involved are very different for the S paths compared with the P paths, so we have different illuminations, and may avoid illumination holes in the images and thereby improve subsequent P-wave imaging with this enhanced velocity model (e.g., Figure 27). Alternatively, the shear mode contamination can be modeled, migrated, and then adaptively subtracted from the final real-data image.

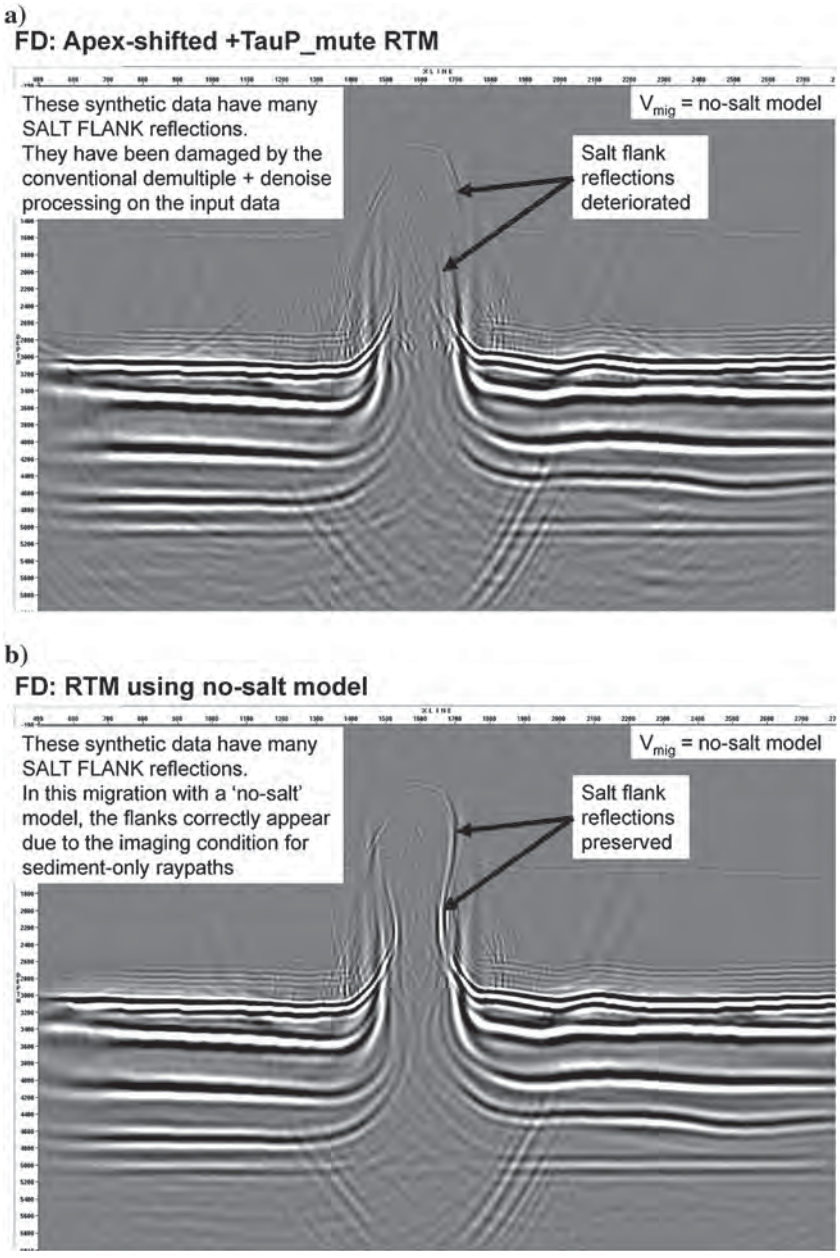

Figure 23. (a) RTM image with inappropriate conventional preprocessing — the steep-sided salt wall is missing, as the preprocessing has removed the some important data that can be used to image the salt (in this case, the apex shifted events seen in the CMP gathers) and (b) RTM image with same model without the deleterious preprocessing, in which most of the salt wall is imaged (from Jones, 2008).

Stress and buoyancy effects

In addition to the stress effects in the sediments overlying and adjacent to the salt body, we also have the possibility of anomalous behavior below due to the reduction in overburden stress caused by buoyancy effects. Some authors conclude that the relatively low density of salt compared with its adjacent sediments results in buoyancy forces, which reduce the vertical stress component, which in turn results in lower seismic velocities than otherwise expected for this depth of burial (e.g., Sengupta and Bachrach, 2008). Other authors, however, conclude that the buoyancy related stresses are fairly minimal (<10 MPa) (e.g., Davison et al., 1996). Reduction in velocity can also be observed in overpressured shales (e.g., Ritter, 2010).

At the level of the base salt, and adjacent to diapirs, we often have a salt weld, in which the salt thickness has thinned to almost zero. In these regions, we have a pronounced increase in stress (due to the comparative lack of buoyant uplift compared with adjacent salt pillows), which tends to locally increase the seismic velocity in the surrounding sedimentary strata (e.g., Hoetz et al., 2011). Often, this is not accounted for in the depth migration velocity model because the scale

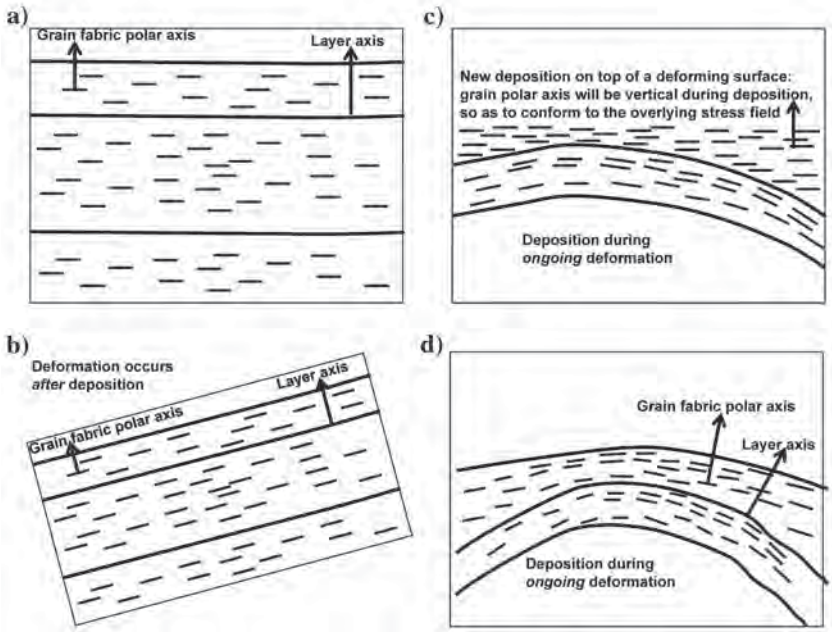

Figure 24. (a) Orientation of platy minerals (or diagenetic mineralization) will parallel the underlying bedding, (b) with subsequently deformation the polar axis of the mineral grains will still be conformable to the bedding axis. However, if the underlying strata are being continuously deformed during deposition, (c) then the grains will initially be deposited locally flat lying, with a vertical polar axis, and (d) but this will be tilted by further ongoing deformation.

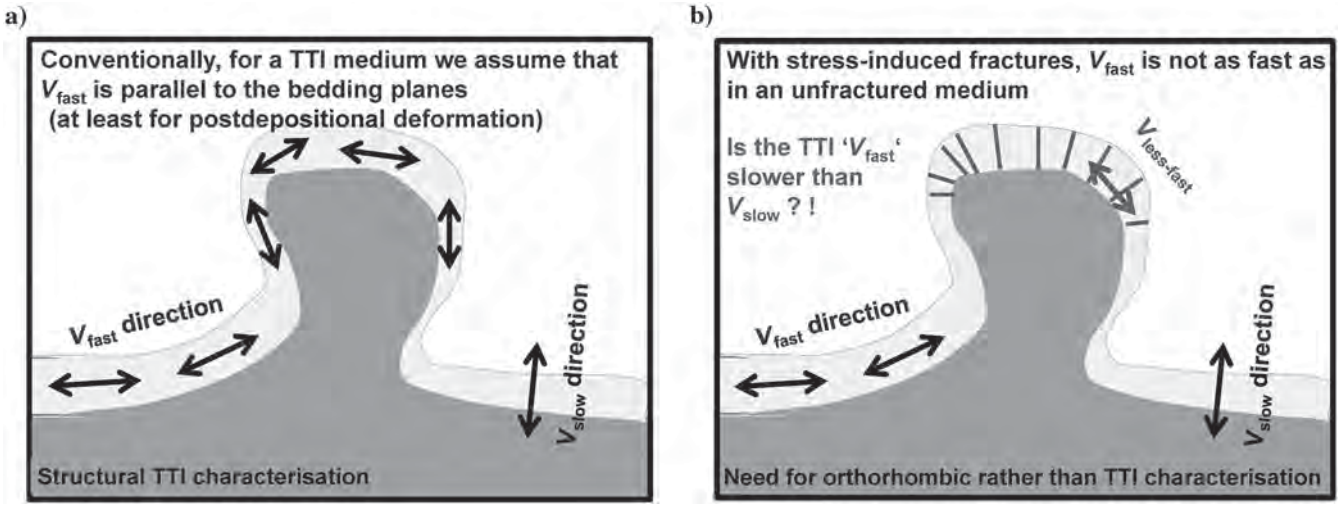

Figure 25. (a) For a TTI description, the fast direction is nominally parallel to the bedding planes, or at least related to them and (b) if we have fracture sets orthogonal to the bedding planes, then this will slow down sound propagation along the beds, and an orthorhombic description of anisotropy may be better suited to describe the problem.

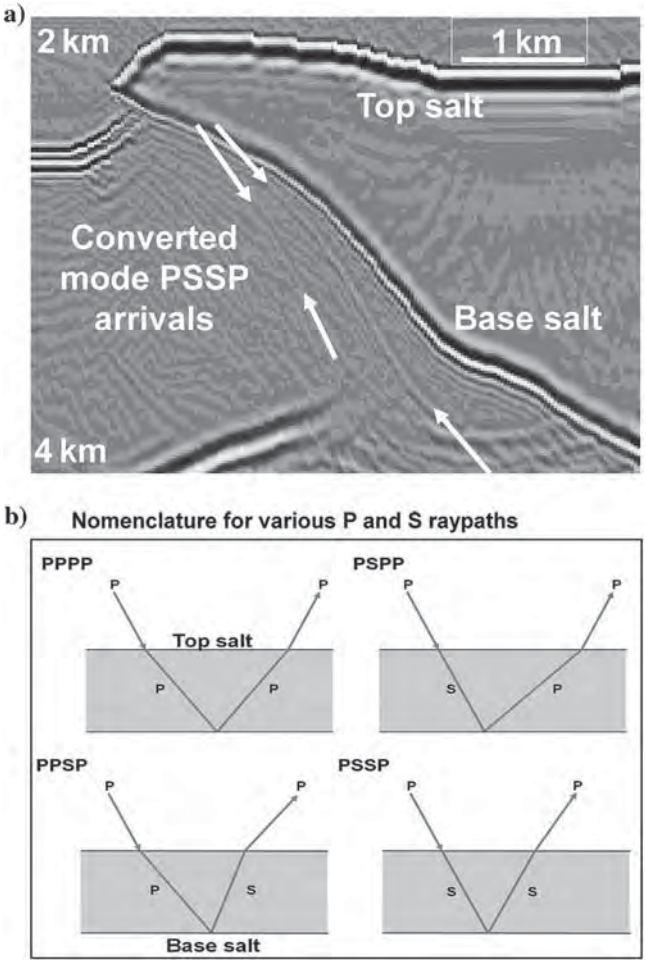

Figure 26. (a) Converted mode reflections from the base salt give misleading images on the P-wave migrated result (from Lafond et al., 2003). The arrows indicate mode converted events and (b) four possible wave-mode conversions through salt.

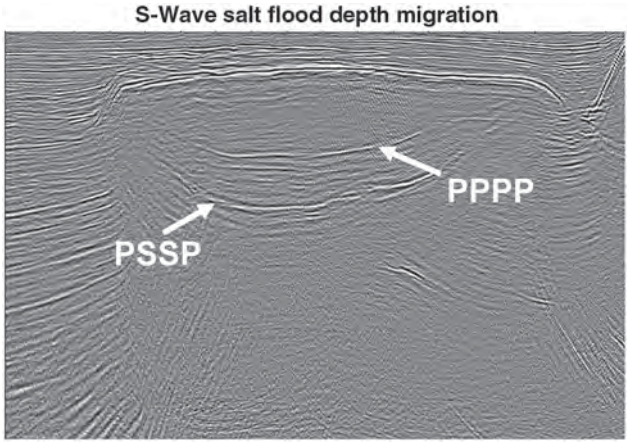

Figure 27. PreSDM performed using S-wave velocity in the salt geobody. This gives us a differently illuminated image of the base salt to assist in its picking. Whereas in a conventional migration with the P-wave salt velocity model, the P-wave base salt image will be in the correct location, and the S-wave image too deep, when we migrate with an S-wave salt velocity, the S-wave image should be at the correct location and the P-wave image too shallow. Picking both can sometimes yield a more complete base salt interpretation.

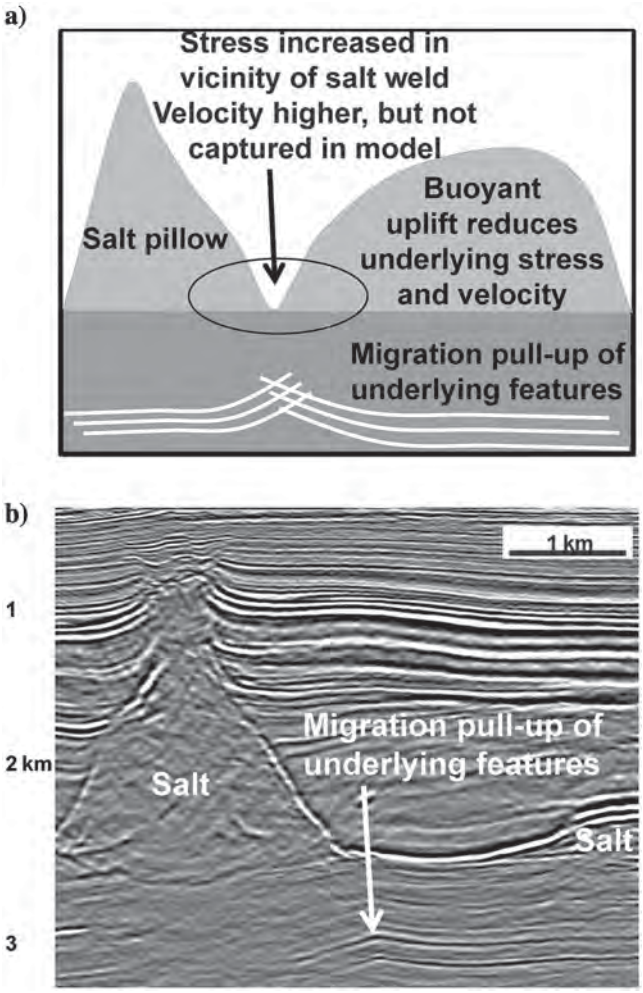

Figure 28. (a) Increased stress at salt welds increases the seismic velocity of the sedimentary rock above and below the weld, but if this is not captured in the velocity model and (b) then pull ups below the weld are observed on depth migrated sections.

length of the effect may be too small to resolve given the depth of the reflectors and available offsets in the seismic data (e.g., Hoetz et al. [2011] mention lateral velocity changes of up to 18% more than 1 km). The velocity used in the migration will, therefore, be too low in the vicinity of the weld and underlying structures will be pulled up on depth-migrated sections. A possible example of this phenomenon can be seen in Figure 28 (courtesy of Harvest Natural Resources).

Conclusions

In the previous examples, we have outlined several pitfalls and problems that can mislead the unwary interpreter or seismic processor when dealing with the seismic imaging of salt bodies. We have not explicitly dealt with the topic of building the velocity depth model itself, but naturally the topics covered in this review must all be taken into account during velocity model building. It is for these reasons that forward modeling studies and rapid migration scenario testing, are especially

useful in ascertaining the degree to which changes in model complexity can alter subsequent interpretation of the resulting images. Recent developments in acquisition and processing to remove source and receiver ghost notches are helping to produce ever better images, including those of salt bodies. However, these advancements in technology can still fall foul of the pitfalls outlined here. Finally, it would be prudent for interpreters to consider these issues when deciding how believable a given image may be, to help derisk their prospect evaluations.

Acknowledgments

We would like to thank J. Leveille, J. Fruehn, J. Brittan, and T. Martin for careful proofreading of this work, the journal's reviewers for their very helpful and constructive suggestions, and ION GX Technology for permission to publish this paper.

References

Baysal, E., D. D. Kosloff, and J. W. C. Sherwood, 1983, Reverse time migration: Geophysics, **48**, 1514–1524, doi: 10.1190/1.1441434.

Bernitsas, N., J. Sun, and C. Sicking, 1997, Prism waves — An explanation for curved seismic horizons below the edge of salt bodies: 59th Annual International Conference and Exhibition, EAGE, Extended Abstracts, E38.

Brauch, W., 1958, On reflected refraction waves: Geophysical Prospecting, **6**, 365–381, doi: 10.1111/j.1365-2478.1958.tb01660.x.

Burliga, S., S. Janiow, and A. Sadowski, 2005, Mining perspectives in the Klodawa Salt Mine considering modern knowledge on tectonics of the Klodawa Salt Structure: Technika Posukiwari Geologicznych Geosnoptyka I Geotermia, **4**, 17–25 (in Polish).

Cao, J., and J. D. Brewer, 2013, Critical reflection illumination analysis: Interpretation, **1**, no. 1, T57–T61, doi: 10.1190/INT-2013-0031.1.

Cavalca, M., and P. Lailly, 2005, Prismatic reflections for the delineation of salt bodies: 75th Annual International Meeting, SEG, Expanded Abstracts, 2550–2553.

Claerbout, J. F., 1985, Imaging the earth's interior: Blackwell Scientific Publications.

Davison, I., G. I. Alsop, and D. J. Blundell, 1996, Salt tectonics: Some aspects of deformation mechanics: Geological Society, London, Special Publications, **100**, 1–10, doi: 10.1144/GSL.SP.1996.100.01.01.

Davison, I., I. Alsop, N. Evans, and M. Safaricz, 2000, Overburden deformation patterns and mechanism of salt diapir penetration: Marine and Petroleum Geology, **17**, 601–618, doi: 10.1016/S0264-8172(00)00011-8.

Davison, I., L. Anderson, and P. Nuttall, 2012, Salt deposition, loading and gravity drainage in the Campos and Santos Salt Basins, Salt tectonics, sediments and prospectivity: Geological Society, London, Special Publications, **363**, 159–174, , doi: 10.1144/SP363.8.

Farmer, P., I. F. Jones, H. Zhou, R. Bloor, and M. C. Goodwin, 2006, Application of reverse time migration to complex imaging problems: First Break, **24**, 65–73.

Faye, J. P., and J. P. Jeannot, 1986, Prestack migration velocities from depth focusing analysis: 56th Annual International Meeting, SEG, Expanded Abstracts, 438–440.

Fletcher, R. F., P. Fowler, P. Kitchenside, and U. Albertin, 2005, Suppressing artifacts in prestack reverse-time migration: 75th Annual International Meeting, SEG, Expanded Abstracts, 2049–2051.

Guitton, A., B. Kaelin, and B. Biondi, 2006, Least-square attenuation of reverse-time migration artifacts: 76th Annual International Meeting, SEG, Expanded Abstracts, 2348–2352.

Hale, D., N. R. Hill, and J. Stefani, 1992, Imaging salt with turning seismic waves: Geophysics, **57**, 1453–1462, doi: 10.1190/1.1443213.

Hemon, C., 1978, Equations d'onde et modeles: Geophysical Prospecting, **26**, 790–821, doi: 10.1111/j.1365-2478.1978.tb01634.x.

Hoetz, G., J. Steenbrinkl, N. Bekkers, A. Vogelaar, and S. Luthi, 2011, Salt-induced stress anomalies: An explanation for variations in seismic velocity and reservoir quality: Petroleum Geoscience, **17**, 385–396, doi: 10.1144/1354-079311-002.

Jackson, C. A. L., and M. W. Lewis, 2012, Origin of an anhydrite sheath encircling a salt diapir and implications for the seismic imaging of steep-sided structures, Egersund Basin, northern North Sea: Journal of the Geological Society, London, **169**, 593–599, doi: 10.1144/0016-76492011-126.

Jones, I. F., 2008, A modeling study of pre-processing considerations for reverse-time migration: Geophysics, **73**, no. 6, T99–T106, doi: 10.1190/1.2981183.

Jones, I. F., 2010, An introduction to velocity model building: EAGE Press.

Jones, I. F., 2012, Tutorial: Incorporating near-surface velocity anomalies in pre-stack depth migration models: First Break, **30**, 47–58, doi: 10.3997/1365-2397.2011041.

Jones, I. F., 2013, Tutorial: The seismic response to strong vertical velocity change: First Break, **31**, 43–54, doi: 10.3997/1365-2397.2013018.

Jones, I. F., M. Sugrue, D. King, M. Goodwin, I. Berranger, H. Zhou, and P. Farmer, 2006, Application of reverse time migration to complex North Sea imaging: Presented at PETEX Biennial Meeting.

Kupfer, D. H., 1976, Shear zones inside Gulf Coast salt stocks help to delineate spines of movement: AAPG Bulletin, **60**, 1434–1447.

Lafond, C., I. F. Jones, M. Bridson, H. Houllevigue, Y. Kerdraon, and J. Peliganga, 2003, Imaging deep water salt bodies in West Africa: The Leading Edge, **22**, 893–896, doi: 10.1190/1.1614155.

Landrø, M., C. Puigdefabregas, and B. Arntsen, 2011, Anisotropy in the salt outcrop at Cardona, Catalonia — Implications for seismic imaging: First Break, **29**, 41–45, doi: 10.3997/1365-2397.2011022.

Leveille, J. P., I. F. Jones, Z-Z. Zhou, B. Wang, and F. Liu, 2011, Subsalt imaging for exploration, production and development: A review: Geophysics, **76**, no. 5, WB3–WB20, doi: 10.1190/geo2011-0156.1.

Lewis, J., 2006, The potential of mode-converted waves in salt interpretation: Presented at SEG/EAGE Summer Research Workshop.

Li, Y., 2012, Velocity model building for tilted orthorhombic depth imaging: 82nd Annual International Meeting, SEG, Expanded Abstracts, doi: 10.1190/segam2012-1231.1.

Liu, F., G. Zhang, S. A. Morton, and J. P. Leveille, 2011, An effective imaging condition for reverse-time migration using wavefield decomposition: Geophysics, **76**, no. 1, S29–S39, doi: 10.1190/1.3533914.

Loewenthal, D., P. L. Stoffa, and E. L. Faria, 1987, Suppressing the unwanted reflections of the full wave equations: Geophysics, **52**, 1007–1012, doi: 10.1190/1.1442352.

McCann, D., A. Comas, G. Martin, A. McGrail, and J. Leveille, 2012, Seismic data processing empowers interpretation: A new methodology serves to mesh processing and interpretation: Hart's E&P, http://www.epmag.com/item/Seismic-Data-Processing-Empowers-Interpretation_94139, accessed 1 October 2014.

McMechan, G. A., 1983, Migration by extrapolation of time-dependent boundary values: Geophysical Prospecting, **31**, 413–420, doi: 10.1111/j.1365-2478.1983.tb01060.x.

Muelhberger, W. R., and P. S. Clabaugh, 1968, Internal structure and petrofabrics of Gulf Coast salt domes, *in* J. Brawnstein, and G. D. O'Brien, eds., Diapirism and diapirs: AAPG Memoir 8, 90–99.

Pratt, R. G., Z.-M. Song, P. Williamson, and M. Warner, 1996, Two-dimensional velocity models from wide-angle seismic data by wavefield inversion: Geophysical Journal International, **124**, 323–340, doi: 10.1111/j.1365-246X.1996.tb07023.x.

Raymer, D. G., J.-M. Kendall, M. C. Beaudoin, M. C. Mueller, and R. R. Kendall, 1999, Measuring the anisotropy of salt in the Mahogany oil field, Gulf of Mexico: AAPG International Conference and Exhibition, 100–103.

Raymer, D. G., A. Tomassi, and J.-M. Kendall, 2000, Predicting the seismic implications of salt anisotropy using numerical simulations of halite deformation: Geophysics, **65**, 1272–1280, doi: 10.1190/1.1444818.

Rickett, J., and P. Sava, 2002, Offset and angle-domain common image-point gathers for shot-profile migration: Geophysics, **67**, 883–889, doi: 10.1190/1.1484531.

Ritter, G., 2010, Using interpretation-driven velocity model building to improve subsalt imaging: 80th Annual International Meeting, SEG, Expanded Abstracts, 4098–4102.

Sava, P., and S. Fomel, 2003, Angle-domain common-image gathers by wavefield continuation methods: Geophysics, **68**, 1065–1074, doi: 10.1190/1.1581078.

Sava, P., and S. Fomel, 2006, Time-shift imaging condition in seismic migration: Geophysics, **71**, no. 6, S209–S217, doi: 10.1190/1.2338824.

Schachl, E., 1987, Nidersachsen-Reidel potash and salt mine of the Kali und Salz AG, shaft Riedel. Zechstein stratigraphy and internal structure of the salt dome of Wathlingen-Haningsen, *in* J. Kulick, and J. Paul, eds., Zechstein in salt sequences and core displays: International Symposium Zechstein, 1, 69–100.

Sengupta, M., and R. Bachrach, 2008, Velocity updating around salt bodies using stress modeling solutions and non-linear elasticity: 78th Annual International Meeting, SEG, Expanded Abstracts, 3048–3052.

Valler, V., J. Morante-Gout, G. Mikkelsen, J. Fruehn, and E. Jenner, 2012, Offset vector tile anisotropic tomography and PreSDM of the Hild OBC: 74th Annual International Conference and Exhibition, EAGE, Extended Abstracts, W007.

Van Gent, H., J. L. Urai, and M. de Keijzer, 2011, The internal geometry of salt structures a first look using 3D seismic data from the Netherlands: Journal of Structural Geology, **33**, 292–311, doi: 10.1016/j.jsg.2010.07.005.

Whitmore, N. D., 1983, Iterative depth migration by backward time propagation: 53rd Annual International Meeting, SEG, Expanded Abstracts, 382–385.

Yoon, K., and K. J. Marfurt, 2006, Reverse-time migration using the Poynting vector: Exploration Geophysics, **37**, 102–107, doi: 10.1071/EG06102.

Yoon, K., K. J. Marfurt, and W. Starr, 2004, Challenges in reverse-time migration: 74th Annual International Meeting, SEG, Expanded Abstracts, 1057–1060.

Zdraveva, O., 2012, Anisotropic model building in complex media: VTI, TTI, or orthorhombic: Presented at SEG/EAGE Summer Research Workshop.

Zhou, H., G. Zhang, and R. Bloor, 2006, Anisotropic acoustic wave equation for VTI media: 68th Annual International Conference and Exhibition, EAGE, Extended Abstracts, H033.

Ian F. Jones received a joint honors B.S. in physics with geology from the University of Manchester, an M.S. in seismology from the University of Western Ontario, and a Ph.D. (1985) in geophysical signal processing from the University of British Columbia. He was the senior geophysical advisor for ION GX Technology in their UK office from 2000 until 2013 when he was made a distinguished advisor. Prior to that, he worked in signal processing research for CGG in their London and Paris offices, latterly as manager of the depth imaging research group. He is an associate editor for the journals GEOPHYSICS and *Geophysical Prospecting*, he teaches the EAGE/SEG continuing education course on velocity model building, and is an external lecturer at Imperial College London and at the University of Leeds. He was awarded the EAGE's Anstey Medal in 2003 for contributions to depth imaging literature and was named the SEG European Honorary Lecturer in 2012. His research interests include velocity model building and migration, and his most recent activities include writing the textbook *An Introduction to Velocity Model*

Building published by EAGE in 2010 and coediting the SEG Geophysics Reprints Series volumes *Classics of Elastic Wave Theory* and *Prestack Depth Migration and Velocity Model Building*.

Ian Davison was a university lecturer in Salvador, Brazil, and Royal Holloway, University of London for 15 years, and he has published more than 70 scientific papers. He is currently the managing director of Earthmoves and GEO International Ltd., two UK-based geologic consultancies specializing in frontier exploration in Africa and Latin America, which have provided services to more than 140 oil and gas exploration companies over the past 20 years. He is a visiting professor at Royal Holloway, and regularly holds technical workshops on salt tectonics and frontier oil exploration for companies all around the world.